

When Sharpening Becomes Collapse: Sampling Bias and Semantic Coupling in RL with Verifiable Rewards

Mingyuan Fan¹ Weiguang Han² Daixin Wang² Cen Chen¹ Zhiqiang Zhang² Jun Zhou²

Abstract

Reinforcement Learning with Verifiable Rewards (RLVR) is a central paradigm for turning large language models (LLMs) into reliable problem solvers, especially in logic-heavy domains. Despite its empirical success, it remains unclear whether RLVR elicits novel capabilities or merely sharpens the distribution over existing knowledge. We study this by formalizing over-sharpening, a phenomenon where the policy collapses onto limited modes, suppressing valid alternatives. At a high level, we discover finite-batch updates intrinsically bias learning toward sampled modes, triggering a collapse that propagates globally via semantic coupling. To mitigate this, we propose inverse-success advantage calibration to prioritize difficult queries and distribution-level calibration to diversify sampling via a memory network. Empirical evaluations validate that our strategies can effectively improve generalization.

1. Introduction

Reinforcement learning with verifiable rewards (RLVR) has become a cornerstone approach for specializing large language models (LLMs) to domains where correctness is checkable (DeepSeek-AI, 2025; Yang et al., 2025). However, there is still no clear consensus on what RLVR fundamentally does to LLMs. One line of work credits RLVR with unlocking new capabilities in LLMs, pointing to emergent chain-of-thought reasoning and strong performance on challenging benchmarks. On the other hand, recent empirical studies (Karan & Du, 2025; Yue et al., 2025; Song et al., 2025) paint a more conservative picture: when given sufficiently large sampling budgets, pre-trained models can often match or even surpass the performance of RL-fine-tuned counterparts. These observations suggest that, rather than endowing models with new skills, RLVR may primarily act

to sharpen the output distribution, making the model more confident in its existing knowledge.

We argue that these perspectives are not mutually exclusive. From a distributional perspective, pre-training and supervised fine-tuning (SFT) provide the model with a rich, low-dimensional manifold of knowledge and latent reasoning procedures. RLVR then performs a search over this manifold, guided by verifiable rewards. A moderate degree of sharpening can be beneficial, since it shifts probability mass toward high-reward semantic modes, making the model more reliable under finite sampling. However, if sharpening is too aggressive, the policy will collapse onto a narrow set of modes, a failure mode we call over-sharpening. Wherein, the model explores only a small subset of the solution space for each input and many valid modes are discarded. As a result, the training process stops discovering new reasoning strategies, limiting capability growth.

This paper is most closely related to research on entropy collapse. Typical examples include flexible clipping ranges (e.g., DAPO-syle methods (Yu et al., 2025; Wu et al., 2025)), as well as token-level heuristics that only update high-entropy tokens (Wang et al., 2025) or truncate gradients on highly confident tokens (Cui et al., 2025). Another family of methods operates at the batch level, discarding degenerate batches (those that are all-correct or all-incorrect) and focusing on medium-difficulty queries, sometimes augmented with carefully constructed synthetic data to keep training in a higher-entropy regime. Other methods directly add entropy regularization or its variants (Cheng et al., 2025; Prabhudesai et al., 2025) to the RL objective. All of these works share a common idea: entropy is a finite resource that must be prevented from diminishing excessively. However, a comprehensive understanding of how RLVR reshapes the solution space remains unclear. To fill this gap, we study the following critical question:

Can we give a formal account of how RLVR reshapes the solution space and characterize the transition from moderate sharpening to over-sharpening that destroys diversity and capabilities?

We identify two mechanisms that drive over-sharpening in RLVR, namely sampling bias and semantic coupling.

¹School of Data Science&Engineering, East China Normal University ²Ant Group. Correspondence to: Cen Chen <cenchen@dase.ecnu.edu.cn>.

First, practical constraints force us to sample only a small number of responses per query during training. These samples are typically drawn from high-probability modes, and therefore cover only a subset of all valid solutions. This biases the model updates toward reinforcing those modes and gradually drives the policy to collapse on them. Second, because model parameters are shared across inputs, updates from one sample affect the behavior on other samples, i.e., semantic coupling. Thus, semantic coupling causes collapse at one point to propagate to semantically related queries. Over time, the effective solution space for many inputs shrinks, the model gains little new information from additional RLVR steps, and collapse is further reinforced. Section 2 analyzes these mechanisms in detail, both theoretically and empirically.

To counteract these, we develop two complementary techniques that act on different parts of the RLVR pipeline. At the learning level, we adjust how much each sampled trajectory influences the update so that easy, already-solved queries do not dominate the optimization signal. At the sampling level, we tune which trajectories are even considered for training so that the model is not repeatedly trained on the same high-probability patterns and is encouraged to explore alternative reasoning paths. Together, these mechanisms can effectively keep RLVR in a moderate sharpening regime, making the model more decisive where it matters, while avoiding the collapse of diverse, potentially useful behaviors. Our contributions can be summarized as follows:

- **A formal framework of sharpening in RLVR.** We formalize the distinction between moderate and over-sharpening and show that, in an ideal infinite-sample setting, the standard RLVR objective does not suppress correct behaviors. We then analyze the realistic finite-batch regime and reveal how sampling bias and shared parameters conspire to suppress unsampled modes and propagate collapse across semantically related queries. This yields a unified picture of when RLVR behaves as a benign sharpening mechanism and when it risks destroying useful diversity.
- **Two simple, general-purpose calibration strategies for RLVR.** Building on this analysis, we introduce inverse-success advantage calibration and distribution-level calibration. The former one automatically down-weights updates from easy, high-success queries and emphasizes harder ones. The later one employ a memory network to reshape the rollout distribution to avoid over-training on already dominant modes and to promote exploration of alternative reasoning patterns. Both techniques can be plugged into existing RLVR pipelines against over-sharpening.
- **Extensive experiments over multiple LLMs and benchmark datasets.** The performance of the proposed meth-

ods over six mathematical reasoning benchmarks consistently outperforms state-of-the-art baselines across both AVG@8 and PASS@8. We also show that our methods are compatible with existing entropy-regularization techniques (e.g., DAPO), delivering additive performance improvements.

2. Analyzing Distribution Collapse: Sampling Bias and Semantic Coupling

2.1. Problem Setup

We consider a policy model π_θ initialized from a reference model π_{ref} . To facilitate analysis, we abstract the output space of the policy model for a given query q as a set of $K_1 + K_2$ mutually exclusive modes: K_1 distinct correct modes $\mathcal{O}^+ = \{o_1, \dots, o_{K_1}\}$ and K_2 distinct incorrect modes $\mathcal{O}^- = \{o_{K_1+1}, \dots, o_{K_1+K_2}\}$. We focus on a classic RLVR scenario with binary verifiable rewards where all correct modes share a non-negative advantage $A_+ \geq 0$, while all incorrect modes share a negative advantage $A_- < 0$. Definition 2.1 formalizes two possible behaviours of an updated policy relative to π_{ref} .

Definition 2.1. A policy π_{new} exhibits moderate sharpening if the probability of every correct mode increases (i.e., $\pi_{\text{new}}(o|q) \geq \pi_{\text{ref}}(o|q)$ for all $o \in \mathcal{O}^+$), and over-sharpening if the probability of any correct mode decreases.

Intuitively, moderate sharpening reflects a holistic improvement where the model becomes more confident in correct modes without forgetting any valid reasoning patterns. Over-sharpening instead suppresses some correct modes in favor of others, which could be problematic because the suppressed patterns might be essential for solving other queries. Consequently, such suppression could harm the model’s generalization ability. Besides, to some extent, over-sharpening can serve as a formal characterization of entropy collapse. As suppression intensifies, the policy degenerates into a deterministic distribution. Thus, entropy collapse is the asymptotic limit of severe over-sharpening. In what follows, we first present that infinite-sample RLVR always yields moderate sharpening, then show how finite-batch sampling fundamentally alters this behavior and leads to over-sharpening on other queries via semantic coupling.

2.2. Sampling Bias

Infinite-sample sharpening behavior. We begin with the standard KL-regularized RL objective:

$$\max_{\theta} \mathbb{E}_{q \sim \mathcal{D}} [\mathbb{E}_{o \sim \pi_\theta(\cdot|q)} [A(q, o)] - \beta D_{KL}(\pi_\theta(\cdot|q) \parallel \pi_{\text{ref}}(\cdot|q))], \quad (1)$$

where \mathcal{D} is the query distribution, $A(q, o)$ is the advantage of o , and $\beta \geq 0$ is the regularization coefficient. Theorem 2.1

Table 1. Summary of our theoretical findings.

Aspect	Key findings
Infinite-sample Regime	The ideal KL-regularized RLVR objective provably yields moderate sharpening, where the probability of every correct mode is strictly increased (Corollary 2.1).
Sampling Bias (Finite-batch)	Collapse is triggered when the model becomes confident (i.e., $\Delta_\pi > 0$), causing the partition function to explode ($Z'(q) > 1$). This forces the suppression of all unsampled correct modes (Theorem 2.3).
Semantic Coupling	Updates do not remain local. The probability mass at q' is disproportionately drawn toward the batch-seen mode at q , thereby suppressing unseen but correct modes for q .

provides the closed-form optimal solution of Equation (1).

Theorem 2.1. *The maximizer of Equation (1), denoted as π^* , is given by*

$$\pi^*(o|q) = \frac{1}{Z(q)} \pi_{\text{ref}}(o|q) \exp\left(\frac{A(q, o)}{\beta}\right), \quad (2)$$

where $Z(q)$ is the partition function ensuring normalization. See Section A for proof.

Then, this optimal policy guarantees moderate sharpening:

Corollary 2.1. *Suppose $A(q, o_i) = A_+ \geq 0$ for $i = 1, \dots, K_1$ and $A(q, o_j) = A_- \leq 0$ for $i = K_1 + 1, \dots, K_1 + K_2$, then Equation (2) yields moderate sharpening.*

Proof. From Equation (2), for $i \in \mathcal{O}^+$, $\pi^*(o_i|q) = \pi_{\text{ref}}(o_i|q) e^{A_+/\beta} / Z(q)$. Since $A_+ \geq 0$, we have $e^{A_+/\beta} \geq 1$. Moreover, $Z(q) = \sum_{i \in \mathcal{O}^+} \pi_{\text{ref}}(o_i|q) e^{A_+/\beta} + \sum_{j \in \mathcal{O}^-} \pi_{\text{ref}}(o_j|q) e^{A_-/\beta} \leq e^{A_+/\beta} \leq 1$ because $e^{A_-/\beta} \leq 1$. Thus $\pi^*(o_i|q) \geq \pi_{\text{ref}}(o_i|q)$ for $i \in \mathcal{O}^+$. \square

Corollary 2.1 indicates that, in the idealized infinite-sample regime, Equation (1) never suppresses a correct mode.

Finite-sample sharpening behavior. In practice, we approximate Equation (1) using Monte Carlo estimation with a finite batch of G independent samples $\{o^{(1)}, \dots, o^{(G)}\} \sim \pi_\theta(\cdot|q)$. This yields the empirical objective:

$$\begin{aligned} \hat{J}(\theta) &= \frac{1}{G} \sum_{s=1}^G A(q, o^{(s)}) \log \pi_\theta(o^{(s)}|q) \\ &\quad - \beta D_{\text{KL}}(\pi_\theta(o^{(s)}|q) \parallel \pi_{\text{ref}}(o^{(s)}|q)). \end{aligned} \quad (3)$$

While gradient descent updates the policy incrementally, the update direction effectively pushes the model towards the stationary point of Equation (3). That stationary point, which we call the batch-optimal policy $\hat{\pi}$, admits a closed form analogous to Theorem 2.1, but with each advantage weighted by the empirical frequency of the corresponding output in the batch. Let N_i denote the number of times mode o_i appears in the batch ($\sum_i N_i = G$). Theorem 2.2 gives the batch-optimal policy $\hat{\pi}$.

Theorem 2.2. *The policy that maximizes Equation (3) is*

$$\hat{\pi}(o_i|q) = \frac{1}{Z'(q)} \pi_{\text{ref}}(o_i|q) \exp\left(\frac{N_i A(q, o_i)}{\beta G}\right), \quad (4)$$

where $Z'(q) = \sum_j \pi_{\text{ref}}(o_j|q) \exp(N_j A(q, o_j) / (\beta G))$.

We emphasize that a single gradient step will generally not reach $\hat{\pi}$ exactly, but the update can be viewed as a geometric interpolation between the current policy and the batch-optimal target (see Theorem B.1), so the qualitative insights carry over.

To understand whether Equation (4) leads to moderate sharpening or over-sharpening, we examine $\Delta_i = \hat{\pi}(o_i|q) - \pi_{\text{ref}}(o_i|q)$ in which $\sum_i \Delta_i = 0$. We partition the modes ($\mathcal{O}^+ \cup \mathcal{O}^-$) into three categories based on empirical frequency N_i and advantage sign $A(q, o_i)$. We first distinguish between sampled modes ($N_i > 0$) with positive versus negative advantages. Following the logic of Corollary 2.1, probability mass is naturally reallocated towards sampled modes with positive advantages, while those with negative advantages are suppressed. The key difference lies in the behavior of unsampled modes ($N_i = 0$).

For any unsampled mode o_i with $N_i = 0$, the exponential term in Equation (4) becomes 1. Consequently, the update simplifies to a uniform scaling:

$$\hat{\pi}(o_i|q) = \frac{\pi_{\text{ref}}(o_i|q)}{Z'(q)} \implies \Delta_i = \pi_{\text{ref}}(o_i|q) \left(\frac{1}{Z'(q)} - 1 \right).$$

This equation implies all unsampled modes move in the same direction. If $Z'(q) > 1$, the probabilities of all unsampled modes decrease, and vice versa. Since the set of unsampled modes could include correct answers, the condition $Z'(q) > 1$ can lead to over-sharpening at q .

Theorem 2.3. *Let S^+ and S^- denote the index sets of sampled correct and incorrect modes, respectively. Then the batch partition function $Z'(q)$ in Theorem 2.2 satisfies:*

$$\begin{aligned} Z'(q) &\geq 1 + \frac{1}{\beta G} \left[A_+ \sum_{i \in S^+} N_i \pi_{\text{ref}}(o_i | q) \right. \\ &\quad \left. - |A_-| \sum_{j \in S^-} N_j \pi_{\text{ref}}(o_j | q) \right]. \end{aligned}$$

Moreover, consider normalized binary advantages $A_+ = \frac{1-p^+}{\sigma}$, $A_- = -\frac{p^+}{\sigma}$, where p^+ is the empirical batch accuracy defined by $\sum_{i \in S^+} N_i = Gp^+$, and $\sigma > 0$ is the empirical standard deviation. Define $\pi_{\min}^+ = \min_{i \in S^+} \pi_{\text{ref}}(o_i | q)$, $\pi_{\max}^- = \max_{j \in S^-} \pi_{\text{ref}}(o_j | q)$, and $\Delta_\pi = \pi_{\min}^+ - \pi_{\max}^-$. The above bound can be simplified to:

$$Z'(q) \geq 1 + \frac{p^+(1-p^+)}{\beta\sigma} \Delta_\pi.$$

See Section C for proof.

We now analyze $Z'(q)$. As shown in Theorem 2.3, the sharpening behavior is primarily governed by the probability gap $\Delta_\pi = \pi_{\min}^+ - \pi_{\max}^-$. Whenever $\Delta_\pi > 0$, we see $Z'(q) > 1$ and therefore a uniform suppression of unsampled modes. Intuitively, $\Delta_\pi > 0$ arises when the model is already performing well on the given query. In fact, this also explains many existing methods (e.g., filtering out high-confidence/easy samples (Xiong et al., 2025; Amin et al., 2025)) as implicit ways of preventing $Z'(q)$ from becoming too large.

Moreover, we observe that the normalization coefficient, $\frac{p^+(1-p^+)}{\sigma}$, acts as a stabilizer by vanishing as $p^+ \rightarrow 0$ or $p^+ \rightarrow 1$, thereby down-weighting updates from highly skewed batches. However, it is insufficient. In other words, the standard normalization indeed can reduce the rate of collapse but fails to address the underlying structural cause, i.e., once the policy becomes confident ($\Delta_\pi > 0$), the optimization landscape fundamentally favors the suppression of diverse, unvisited modes.

2.3. Semantic Coupling

We now study how over-sharpening at a query q affects the model's behavior at another query q' . We focus on the case where q and q' are positively semantically related, e.g., two math problems that rely on the same underlying theorem. This implies that a parameter update improving the model's performance on q should also increase the likelihood of the correct response for q' . We absorb the sign of the advantage $A(q, o)$ into the gradient direction and formalize this in Assumption 2.1.

Assumption 2.1. Let (q, o) and (q', o') be two query–output pairs that are positively semantically related. We assume that their logit gradients are non-negatively aligned:

$$\nabla_\theta f(q, o)^\top \nabla_\theta f(q', o') \geq 0.$$

Recall from Theorem 2.2 that the batch-optimal policy $\hat{\pi}$ for q implies a target logit shift. Let $\mathbf{y} \in \mathbb{R}^G$ be the vector of target shifts for the batch $\{o^{(s)}\}_{s=1}^G$, where $y_i = \frac{N_i |A(q, o_i)|}{\beta G} \mathbf{1}$.

¹Due to the sign-absorption convention, the advantage term takes its absolute value here.

The parameter update $\Delta\theta$ induced by fitting this batch (Jacot et al., 2018) is given by²:

$$\Delta\theta = \mathbf{J}_q^\top (\mathbf{J}_q \mathbf{J}_q^\top)^{-1} \mathbf{t} = \mathbf{J}_q^\top \mathbf{K}_{qq}^{-1} \mathbf{y},$$

where \mathbf{J}_q is the Jacobian of the logits with respect to parameters, and $\mathbf{K}_{qq} = \mathbf{J}_q \mathbf{J}_q^\top$ is the empirical kernel matrix on the current batch.

For (q', o') , the change in the logit value is induced by the parameter update $\Delta\theta$:

$$\Delta f(q', o') = \nabla_\theta f(q', o')^\top \Delta\theta = \mathbf{k}_{q'}^\top \mathbf{K}_{qq}^{-1} \mathbf{y},$$

where $\mathbf{k}_{q'}$ is the kernel vector with entries $[\mathbf{k}_{q'}]_i = k((q', o'), (q, o^{(i)})) \triangleq \nabla_\theta f(q', o')^\top \nabla_\theta f(q, o^{(i)})$.

We define $\lambda_{\min}, \lambda_{\max} = \min_i K_{ii}, \max_i K_{ii}$ (feature specificity) and $\rho_{\min}, \rho_{\max} = \min_{i \neq j} K_{ij}, \max_{i \neq j} K_{ij}$ (cross-similarity). We also introduce Assumptions 2.2 and 2.3. First, to render the analysis tractable, we model the shift from a source query to a target query as a signal decay, where gradient correlations are naturally attenuated³. Second, we enforce a locality condition, reflecting the intuition that a parameter update intended to reinforce a mode o should boost o itself significantly more than it boosts distinct modes o' . We then obtain the bound on the induced logit shifts, as shown in Theorem 2.4.

Assumption 2.2. We assume that gradient correlations decay by a factor $\eta \in [0, 1]$ when shifting from q to q' , i.e., $k((q', o'), (q, o^{(s)})) \approx \eta K((q, o'), (q, o^{(s)}))$.

Assumption 2.3. We assume that $\lambda_{\min} \geq \rho_{\max}$, suggesting that the self-alignment consistently exceeds cross-alignment.

Theorem 2.4. Let $\mathcal{A}_{\text{sum}} \triangleq \sum_{i=1}^G y_i$. The induced logit shift $\Delta f(q', o')$ satisfies the following bounds based on whether o' appears in the training batch $\{o^{(i)}, i = 1, \dots, G\}$:

- If $o' \notin \{o^{(i)}\}$, the logit increase is upper-bounded by:

$$\Delta f(q', o') \leq \frac{\eta \rho_{\max} \mathcal{A}_{\text{sum}}}{\lambda_{\min} + (G-1)\rho_{\min}}.$$

- If $o' = o^{(i)}$ for some $i \in \{1, \dots, G\}$, the logit increase is lower-bounded by

$$\Delta f(q', o') = \Delta f(q', o_i) \geq \frac{\eta N_{o'} (\lambda_{\min} - \rho_{\min})}{\lambda_{\max} - \rho_{\max}} (y_k - \frac{\rho_{\max} \mathcal{A}_{\text{sum}}}{\lambda_{\max} + (G-1)\rho_{\max}}).$$

²For readers unfamiliar with the optimization dynamics in the linearized regime, we provide the necessary background in Section D.

³In fact, Assumption 2.2 can be relaxed to a bounded interval $[\eta_{\min}, \eta_{\max}]$ for greater generality, which would simply introduce a scaling factor $\frac{\eta_{\min}}{\eta_{\max}}$ to the ratio derived in Corollary 2.2.

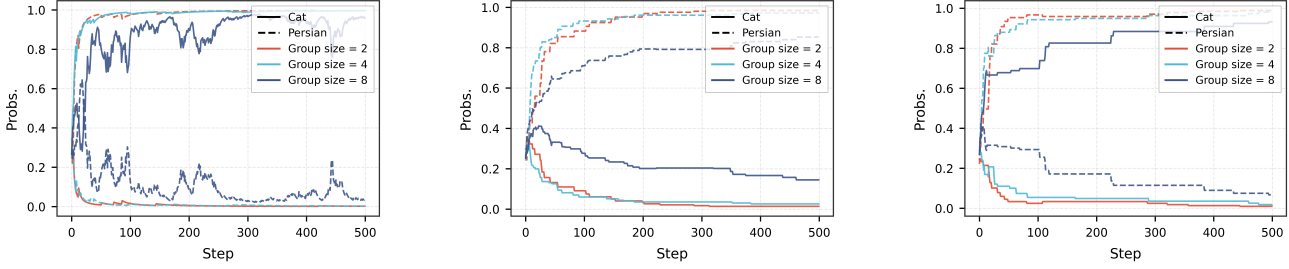


Figure 1. Effect of advantage estimation and group size on over-sharpening. Probability of Cat and Persian over training for raw (left), mean-shifted (mid), and normalized (right) advantages.

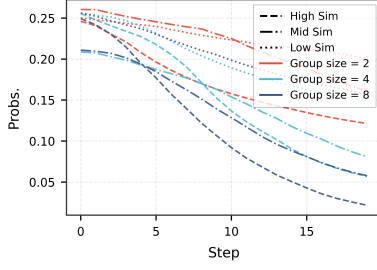


Figure 2. Semantic coupling accelerates collapse. Accuracy on the held-out Siamese class while training only on Persian. Stronger semantic coupling and larger group sizes both lead to faster degradation of Siamese accuracy.

See Section E for proof.

We now leverage Theorem 2.4 to characterize when over-sharpening occurs at q' . Consider a semantically coupled pair (q, q') and suppose that at q' there exists at least one mode o' that appears in the batch for q (Case 2) and at least one mode \bar{o} that does not (Case 1). Over-sharpening at q' arises when the batch-seen mode receives a much larger logit increase than a semantically related but batch-unseen mode, so that after normalization the latter is suppressed. Corollary 2.2 makes this comparison explicit.

Corollary 2.2. Define the ratio \mathcal{R} of the lower bound in Case 2 to the upper bound in Case 1:

$$\mathcal{R} \triangleq \frac{\lambda_{\min} - \rho_{\min}}{\lambda_{\max} - \rho_{\max}} \left[\frac{N_{o'} y_k}{\mathcal{A}_{\text{sum}}} \cdot \left(\frac{\lambda_{\min} + (G-1)\rho_{\min}}{\rho_{\max}} \right) - \frac{\lambda_{\min} + (G-1)\rho_{\min}}{\lambda_{\max} + (G-1)\rho_{\max}} \right].$$

In particular, if $\lambda_{\min} \approx \lambda_{\max} \approx \lambda$ and $\rho_{\min} \approx \rho_{\max} \approx \rho$, \mathcal{R} simplifies to $\left[\frac{N_{o'} y_k}{\mathcal{A}_{\text{sum}}} \left(\frac{\lambda}{\rho} + G - 1 \right) - 1 \right]$. See Section F for proof.

Qualitatively, \mathcal{R} measures how much more strongly a batch-seen mode at q' is pushed compared to a semantically related but unseen mode. A large value of \mathcal{R} means that the guaranteed logit increase of a batch-seen mode at q' dominates the maximum possible increase of a batch-unseen

mode. In this regime, probability mass is pulled disproportionately toward the former, leading to over-sharpening at q' . From the explicit form, over-sharpening is promoted when:

- The update budget is concentrated on a single overlapping mode, i.e., $N_{o'} y_k / \mathcal{A}_{\text{sum}}$ is large.
- Features are highly specific, i.e., λ / ρ is large, so updates align strongly with batch directions and leak little to other modes.
- Effective batch reinforcement is strong, i.e., the batch size G and the number of repeated samples of the same mode are large.

2.4. Empirical Illustration of Over-Sharpening

We use a controlled softmax classification setting to separately probe sampling bias and semantic coupling. We consider two superclasses (Cat, Dog) and two subclasses (Persian, Siamese) with fixed feature embeddings:

$$\mathbf{e}_{\text{Cat}} = [0.5, 0.5, 0.5, 0.1], \mathbf{e}_{\text{Persian}} = [0.75, 0.5, 0.25, 0.1], \\ \mathbf{e}_{\text{Dog}} = [0.1, 0.1, 0.1, 0.9], \mathbf{e}_{\text{Siamese}} = [0.25, 0.5, 0.75, 0.1].$$

Both Persian and Siamese are close to the Cat superclass while differing along their subclass-specific dimensions. In this case, the input embedding plays the role of the query q , and the sampled label plays the role of the output o . We train this classifier with common RLVR algorithms, using a binary verifiable reward and SGD for optimization. We present only Persian inputs for 500 steps. At each step, we sample a group of G labels from the current softmax policy and assign reward 1 if the sampled label is Cat or Persian, and 0 otherwise, i.e., both the superclass and subclass are treated as correct for Persian. We then compute advantages under various methods (raw reward, mean-shifted, and normalized) and update the policy accordingly. We track the probabilities $\pi(o = \text{Cat}|q = \text{Persian})$ and $\pi(o = \text{Persian}|q = \text{Persian})$ for different group sizes G , as shown in Figure 1.

Across all advantage estimators and group sizes, the model eventually collapses onto a single label (either Cat or Per-

sian). Which label wins is random, determined by early sampling noise. Once one mode is sampled more often, it dominates subsequent updates. Increasing G reduces the variance of early updates and thereby delays collapse, but does not prevent it. The choice of the advantage estimator primarily modulates the rate of collapse. Raw rewards lead to the most aggressive over-sharpening, mean-shifted advantages are slightly more conservative, and, normalized advantages slow the process further. This aligns with our theory that normalization (via $p^+(1-p^+)/\sigma$) stabilizes $Z'(q)$. We further evaluate advanced advantage estimators, including RLOO and Reinforce++ with baseline, and observe that while they modulate the convergence rate, the collapse persists. Moreover, momentum and adaptive optimizers (MI, AdamW) typically exacerbate over-sharpening by accumulating past gradients and amplifying early sampling biases, pushing the policy more quickly into the collapsed regime. See Section G for these results.

We next study semantic coupling by measuring how training on Persian affects the held-out Siamese subclass. We keep the training protocol unchanged but now monitor $\pi(o = \text{Siamese} \mid q = \text{Siamese})$ over training. Our theory predicts that the propagation of collapse is governed by \mathcal{R} which grows with group size G and with semantic coupling through the ratio λ/ρ . To modulate semantic coupling, we modify the Siamese embedding:

$$[0.25, 0.5, 0.75, 0.1], [0.1, 0.5, 0.9, 0.1], [0.0, 0.5, 1.0, 0.1],$$

progressively shifting mass from the Persian-specific coordinate (first dimension) to the Siamese-specific coordinate (third dimension). We refer to these as High, Mid, and Low similarity. As can be seen in Figure 2, we observe that the probability of correctly classifying Siamese is strongly squeezed over training. The effect is more severe when similarity is higher (larger shared features) and G is larger. As we increase the overlap between Persian and Siamese features, the empirical ratio λ/ρ estimated from the gradient Gram matrix also increases (details in Section G, which in turn raises \mathcal{R}). The observed faster collapse of Siamese accuracy thus matches the predicted growth in semantic over-sharpening. We highlight that this interaction between group size and semantic coupling is somewhat counterintuitive. Indeed, a larger G is often expected to stabilize training, yet in our RLVR setting, it can worsen over-sharpening and propagate collapse across semantically related classes.

3. Approach

We now introduce two complementary mechanisms designed to keep RLVR in moderate sharpening regime, including inverse-success advantage calibration (IAC) which adjusts how strongly each sampled trajectory contributes to the policy update, and distribution-level calibration (DLC)

which tunes the rollout distribution itself to prevent the policy from repeatedly sampling the same high-probability patterns. Section H presents the full algorithmic pipeline (Algorithm 1), alongside visualizations that show the effectiveness of our methods in mitigating over-sharpening.

3.1. Inverse-success Advantage Calibration (IAC)

Our first strategy targets the mechanism identified in Theorem 2.3: over-sharpening at a query q is driven by an inflated batch-dependent partition function $Z'(q)$, which uniformly suppresses the probabilities of all unsampled modes. Specifically, Theorem 2.3 gives $Z'(q) \geq 1 + \frac{p^+(1-p^+)}{\beta\sigma} [\pi_{\min}^+ - \pi_{\max}^-]$. We find that standard advantage normalization cannot cancel the second term. When the reference model is already confident on positive samples $\pi_{\min}^+ - \pi_{\max}^- > 0$, the right-hand side exceeds 1, causing $Z'(q) > 1$ and aggressive suppression of all unsampled (including correct) modes.

A natural solution would be to reweight advantages inversely proportional to $\pi_{\text{ref}}(\cdot)$ so that high-probability easy positives contribute less. In detail, let $\tilde{A}_k = A(q, o_k)/\pi_{\text{ref}}(o_k)$. Then the lower bound becomes:

$$\begin{aligned} Z'(q) &\geq 1 + \frac{1}{\beta G} \sum_{k=1}^G N_k \tilde{A}_k \pi_{\text{ref}}(o_k) \\ &= 1 + \frac{1}{\beta G} \sum_{k=1}^G N_k \left(\frac{A_k}{\pi_{\text{ref}}(o_k)} \right) \pi_{\text{ref}}(o_k) \\ &= 1 + \frac{1}{\beta G} \sum_{k=1}^G N_k A_k = 1. \end{aligned}$$

In the last line, we use the normalization property $\sum_k N_k A_k = 0$. In practice, however, we observe two issues when directly implementing this calibration:

- **High variance in sequence probabilities.** LLMs exhibit extremely high variance in sequence-level probabilities. After calibration, this variance transfers to the advantages, which in turn causes highly unstable gradient updates.
- **Negative samples are not purely wrong.** Negative samples often contain partially correct reasoning segments or are just being truncated due to a maximum length constraint. Over-amplifying their (negative) advantages can therefore destroy useful intermediate structure and destabilizes training.

As a remedy, we only calibrate the advantages of positive samples, and we do so using an inverse-success heuristic rather than the raw probabilities. For each positive sample, we define the following calibrated advantage:

$$\tilde{A}(q, o_k^+) = A(q, o_k^+) \cdot (G - |S^+|)^\alpha, \alpha \geq 0.$$

Notice that we leave negative samples unmodified, i.e., $\tilde{A}(q, o_k^-) = A(q, o_k^-)$. This design has two key properties:

- $(G - |S^+|)$ serves as a proxy for the difficulty of the query. When positives are rare, the factor is large. Thus, harder queries receive a larger effective weight.
- The exponent α controls the calibration strength. $\alpha = 0$ recovers the uncalibrated baseline, while larger α increases the relative weight of positives from hard queries and de-emphasizes those from easy queries.

Intuitively, this inverse-success calibration redistributes the advantage budget away from queries where the model is already confident and towards queries where success is rare, thereby preventing $Z'(q)$ from becoming excessively large and mitigating over-sharpening of already mastered modes. At the same time, by not amplifying negative samples, we avoid collapsing on partially correct or truncated trajectories.

3.2. Distribution-Level Calibration via Decoupled Sampling (DLC)

While inverse-success calibration moderates how strongly each batch can push $Z'(q)$, it does not address that once certain trajectories have been suppressed and their probabilities become very small, they almost never appear again in subsequent rollouts. This feedback loop, i.e., low probability leading to low sampling frequency, exacerbates sampling bias over time. Thus, our second mitigation is to calibrate the sampling distribution itself.

A vanilla idea would be to increase the sampling temperature of the policy, flattening the distribution. However, a global temperature treats all tokens equally, ignoring that different tokens learn at different speeds and have different difficulty. To address this, we propose a memory-network-based distribution calibration that adapts exploration based on the policy’s rollout history.

In detail, we introduce an auxiliary memory network m_ϕ with logits $f_\phi(q, o)$, trained to approximate the empirical frequency of (q, o) pairs encountered during training process. Concretely, after each training step, we update m_ϕ on the sampled trajectories (with a standard cross-entropy loss) so that it outputs higher logits for frequently generated outputs and lower logits for rarely seen ones.

At sampling time, rather than drawing from the raw policy logits $f_\theta(q, \cdot)$, we construct a calibrated sampling distribution by subtracting the memory logits:

$$\tilde{f}(q, o) = f_\theta(q, o) - \mu \cdot f_\phi(q, o),$$

$$\pi_{\text{sample}}(o | q) \propto \exp(\tilde{f}(q, o)).$$

where $\mu \geq 0$ is a balance factor controlling how strongly the memory prior influences exploration. Intuitively, the memory network acts as a learned frequency prior. Wherein, modes that have been sampled many times receive larger $f_\phi(q, o)$ and are thus down-weighted in $\tilde{f}(q, o)$, while under-explored modes are relatively boosted. From the perspective of Theorem 2.2 and Theorem 2.3, by explicitly discouraging repeated sampling of the same high-probability modes, it prevents any single mode from accumulating a disproportionately large empirical count N_i across updates.

Computational overhead and practical choice. Compared to inverse-success calibration, the memory network is significantly more expensive. For instance, if m_ϕ shares the same architecture as the policy, then in principle we roughly double both training and rollout compute. In our implementation, the dominant additional cost comes from rollout. Although integrated with high-performance backends like vLLM, the absence of kernel-level support for synchronized multi-model sampling results in a $5 \times$ rollout overhead. Given this overhead, our subsequent evaluations mainly use inverse-success advantage calibration as the default mitigation, since it is lightweight. We treat the memory network as an optional, higher-cost augmentation that can further improve performance when compute allows. Empirically, we observe that adding the memory network on top of inverse-success calibration provides additional gains, but for most RLVR scenarios, the advantage-level method alone strikes a better balance between effectiveness and efficiency.

4. Empirical Evaluation

4.1. Experimental Setup

Models, datasets, and metrics. We evaluate our methods in the context of mathematical reasoning with verifiable rewards. We use the DeepScaleR (Luo et al., 2025) corpus as our primary RLVR training set, consisting of approximately 40.3k problem–answer pairs with checkable labels. To assess generalization, we report performance on six diverse benchmarks: GSM8K, AIME 2024, MATH 500, LightEval, Minerva (Lewkowycz et al., 2022), and O-Bench (He et al., 2024). We conduct experiments with three backbone models, Qwen3-4B, Qwen3-8B and Qwen3-14B (Yang et al., 2025). As evaluation metrics, we report PASS@8 and AVG@8. PASS@8 measures the proportion of queries for which at least one of the eight responses is correct, and AVG@8 reflects the average proportion of correct responses per query.

Baselines. We compare our approaches against a range of RL baselines commonly used in LLM training, including GRPO (DeepSeek-AI, 2025), DrGRPO (Liu et al., 2025), RLOO (Kool et al., 2019), Reinforce++ with baseline (Hu et al.), and DAPO (Yu et al., 2025). All baselines are run in

Table 2. AVG@8 (%) performance of various methods across six benchmark datasets.

Model	Method	GSM8K	Math500	LightEval	AIME24	Minerva	O-Bench	Avg.
Qwen3-4B	GRPO	93.72	85.58	<u>70.61</u>	34.58	43.06	<u>48.85</u>	62.73
	RLOO	93.69	86.44	70.24	32.50	43.98	<u>47.91</u>	62.46
	Reinforce++	<u>94.04</u>	85.43	70.21	<u>36.25</u>	<u>45.63</u>	48.57	<u>63.36</u>
	DrGRPO	94.10	83.56	69.54	35.42	45.43	47.83	62.65
	IAC (Ours)	94.63	<u>86.43</u>	72.15	37.08	47.01	48.87	64.36
Qwen3-8B	GRPO	95.59	85.81	71.12	35.42	47.20	49.79	64.16
	RLOO	95.56	86.89	72.30	36.25	46.78	49.74	64.59
	Reinforce++	<u>95.56</u>	<u>87.07</u>	<u>72.14</u>	40.68	<u>47.84</u>	<u>50.30</u>	<u>65.60</u>
	DrGRPO	95.35	86.11	71.56	34.58	47.38	49.87	64.14
	IAC (Ours)	95.72	87.67	73.85	35.42	50.60	50.49	65.63
Qwen3-14B	GRPO	95.96	89.42	73.83	53.45	50.32	55.28	69.71
	RLOO	<u>96.04</u>	90.29	73.64	54.17	50.46	55.10	69.95
	Reinforce++	95.82	90.88	<u>73.96</u>	54.17	<u>50.87</u>	<u>56.00</u>	70.28
	DrGRPO	95.96	90.37	73.85	<u>54.85</u>	50.69	55.35	<u>70.18</u>
	IAC (Ours)	96.36	<u>90.70</u>	74.52	56.67	52.34	56.32	71.15

Table 3. PASS@8 (%) performance of various methods across six math benchmark datasets.

Model	Method	GSM8K	Math500	LightEval	AIME24	Minerva	O-Bench	Avg.
Qwen3-4B	GRPO	96.74	91.94	<u>75.43</u>	47.37	54.54	<u>56.44</u>	70.41
	RLOO	<u>96.98</u>	<u>92.22</u>	75.39	43.65	55.01	<u>56.31</u>	69.93
	Reinforce++	96.45	91.58	74.92	<u>50.54</u>	<u>55.32</u>	56.38	<u>70.87</u>
	DrGRPO	96.43	89.90	73.87	47.02	54.60	55.08	69.48
	IAC (Ours)	97.38	92.33	77.30	52.28	57.74	56.59	72.27
Qwen3-8B	GRPO	96.51	91.39	75.19	52.36	55.65	56.88	71.33
	RLOO	<u>97.25</u>	92.64	76.17	50.92	55.55	57.68	71.70
	Reinforce++	96.96	92.31	75.96	55.24	56.12	<u>57.78</u>	<u>72.40</u>
	DrGRPO	97.11	91.57	75.36	52.25	55.41	57.26	71.49
	IAC (Ours)	97.56	94.54	78.69	52.67	60.60	58.48	73.76
Qwen3-14B	GRPO	97.53	93.75	76.54	70.44	59.40	60.87	76.42
	RLOO	97.43	93.62	76.36	<u>73.18</u>	59.78	61.14	76.92
	Reinforce++	<u>97.79</u>	94.12	<u>76.74</u>	<u>71.71</u>	60.27	<u>61.42</u>	<u>77.01</u>
	DrGRPO	97.53	<u>94.27</u>	76.57	71.83	<u>61.03</u>	60.96	77.03
	IAC (Ours)	98.11	94.37	77.28	78.07	62.64	62.37	78.81

Table 4. Compatibility analysis using Qwen3-8B.

Metric	Method	Math500	LightEval	Minerva	O-Bench
AVG@8	DAPO	87.25	72.04	47.15	50.17
	IAC	87.67	73.85	50.60	50.49
	DAPO+IAC	87.89	74.48	51.07	50.58
	DAPO+IAC+DLC	88.44	75.42	51.90	51.38
PASS@8	DAPO	92.96	76.62	56.38	58.28
	IAC	94.54	78.69	60.60	58.48
	DAPO+IAC	94.74	84.80	61.97	58.88
	DAPO+IAC+DLC	95.19	85.15	62.50	60.12

the same setting with identical reward functions and sampling budgets for fair comparison.

Implementation details. All models are optimized with AdamW using a learning rate of 10^{-6} . We employ a global batch size of 64 and sample $G = 8$ responses per query. Training is run for 2000 steps, and we evaluate checkpoints every 50 steps, reporting the peak performance for each method. We employ VERL’s built-in recipes to standardize the implementation of baseline methods. For IAC, we use $\alpha = 1$ by default. Due to the page limit, we leave sensitivity analysis (α), the comparison with sample-filtering baselines, and the entropy evolution analysis in Section I.

All experiments are conducted using 32 H200 GPUs.

4.2. Evaluation Result

Comparison with state-of-the-art methods. Table 2 and Table 3 summarize the AVG@8 and PASS@8 performance of different methods, respectively, across six mathematical reasoning benchmarks and three Qwen3 backbones. Overall, our method attains the best AVG@8 and PASS@8 in almost all settings across models and datasets, indicating that calibrated sharpening consistently improves both average quality and success probability. In contrast, different baselines occasionally excel on specific benchmarks. For example, Reinforce++ is competitive on AIME24 and MATH500, and RLOO sometimes attains strong averages. To illustrate this in more detail, consider the Qwen3-14B results. Here, all baselines are already strong, yet our method still delivers clear gains. In terms of AVG@8, our method can raise the overall average from roughly 70.2 (Reinforce++ / DrGRPO) to 71.15. For PASS@8, the improvement is more striking: from 77.03 (best baseline) to 78.81. In particular, improvements on harder, less saturated benchmarks (AIME24, Minerva, O-Bench) are more pronounced than on easier ones such as GSM8K, suggesting that our approach

is especially beneficial when reasoning requires exploring multiple reasoning modes rather than amplifying a single dominant pattern. On the smaller backbones Qwen3-4B and Qwen3-8B, we observe a consistent pattern.

Compatibility with other methods. We also evaluate the compatibility of the proposed methods. The results, presented in Table 4, reveal three key insights. First, IAC alone outperforms DAPO on both AVG@8 and PASS@8 metrics across most datasets. Second, when IAC is integrated into DAPO (DAPO+IAC), we observe additive performance gains. For instance, on LightEval (PASS@8), the combination improves performance from 76.62% (DAPO) to 84.80%. Third, we incorporate DLC with a memory network (Qwen3-1.7B) of $\mu = 0.5$ (DAPO+IAC+DLC). This full configuration yields the highest performance.

5. Related Work

Since the release of DeepSeek-R1 (DeepSeek-AI, 2025), RLVR (or GRPO and its variants) has gained particular traction for enhancing the reasoning ability of LLMs. To stabilize the often volatile training dynamics, a significant body of work focused on refining advantage estimation. Prominent techniques include RLOO (Leave-One-Out) (Kool et al., 2019), DrGRPO (Liu et al., 2025), which modifies the variance term to improve stability, and Reinforce++ with baseline (Hu et al.) that shifts from sample-level to global batch-level normalization. Another line of work has identified a critical correlation between model performance and the evolution of policy entropy (Cui et al., 2025). While rapid entropy reduction can accelerate convergence, it drives the model toward premature saturation at local optima. Xiong et al. (2025) highlighted the importance of negative samples in RLVR. Other approaches focus on sustaining entropy to prolong exploration. These methods employ techniques such as safe or flexible clipping mechanisms (Yu et al., 2025; Wu et al., 2025), restricting gradient updates to high-entropy tokens (Wang et al., 2025), or incorporating entropy explicitly as a regularization term (He et al., 2025). However, the field remains divided. Recent empirical studies (Karan & Du, 2025; Yue et al., 2025; Song et al., 2025) indicate that RLVR training can sometimes lead to a degradation in general capabilities.

6. Conclusion

In this work, we formalised the phenomenon of over-sharpening within RLVR framework. We revealed that the very clarity of verifiable rewards, when combined with finite-sample bias and semantic coupling, can lead to a pathological collapse of reasoning diversity. To counter this, we introduced two calibration mechanisms designed to stabilize the RLVR partition function and decouple the sampling

process from the current policy’s modes. We conducted extensive evaluations and showed that these mechanisms substantially mitigate entropy collapse and stabilize generalization in verifiable-reward settings. Future work may extend our analysis to richer reward structures and more complex interaction protocols (e.g., multi-turn tool use), etc.

References

Amin, K., Babakniya, S., Bie, A., Kong, W., Syed, U., and Vassilvitskii, S. Escaping collapse: The strength of weak data for large language model training. *CoRR*, abs/2502.08924, 2025. doi: 10.48550/ARXIV.2502.08924. URL <https://doi.org/10.48550/arXiv.2502.08924>.

Cheng, D., Huang, S., Zhu, X., Dai, B., Zhao, W. X., Zhang, Z., and Wei, F. Reasoning with exploration: An entropy perspective. *CoRR*, abs/2506.14758, 2025. doi: 10.48550/ARXIV.2506.14758. URL <https://doi.org/10.48550/arXiv.2506.14758>.

Cui, G., Zhang, Y., Chen, J., Yuan, L., Wang, Z., Zuo, Y., Li, H., Fan, Y., Chen, H., Chen, W., Liu, Z., Peng, H., Bai, L., Ouyang, W., Cheng, Y., Zhou, B., and Ding, N. The entropy mechanism of reinforcement learning for reasoning language models. *CoRR*, abs/2505.22617, 2025. doi: 10.48550/ARXIV.2505.22617. URL <https://doi.org/10.48550/arXiv.2505.22617>.

DeepSeek-AI. Deepseek-r1: Incentivizing reasoning capability in llms via reinforcement learning. *CoRR*, abs/2501.12948, 2025. doi: 10.48550/ARXIV.2501.12948. URL <https://doi.org/10.48550/arXiv.2501.12948>.

He, A., Fried, D., and Welleck, S. Rewarding the unlikely: Lifting GRPO beyond distribution sharpening. *CoRR*, abs/2506.02355, 2025. doi: 10.48550/ARXIV.2506.02355. URL <https://doi.org/10.48550/arXiv.2506.02355>.

He, C., Luo, R., Bai, Y., Hu, S., Thai, Z. L., Shen, J., Hu, J., Han, X., Huang, Y., Zhang, Y., Liu, J., Qi, L., Liu, Z., and Sun, M. Olympiadbench: A challenging benchmark for promoting AGI with olympiad-level bilingual multimodal scientific problems. In Ku, L., Martins, A., and Srikumar, V. (eds.), *Proceedings of the 62nd Annual Meeting of the Association for Computational Linguistics (Volume 1: Long Papers)*, ACL 2024, Bangkok, Thailand, August 11-16, 2024, pp. 3828–3850. Association for Computational Linguistics, 2024. doi: 10.18653/V1/2024.ACL-LONG.211. URL <https://doi.org/10.18653/v1/2024.acl-long.211>.

Hu, J., Liu, J. K., Xu, H., and Shen, W. Reinforce++: Stabilizing critic-free policy optimization with global normalization. *arXiv preprint arXiv*, 2501.

Jacot, A., Hongler, C., and Gabriel, F. Neural tangent kernel: Convergence and generalization in neural networks. In Bengio, S., Wallach, H. M., Larochelle, H., Grauman, K., Cesa-Bianchi, N., and Garnett, R. (eds.), *Advances in Neural Information Processing Systems 31: Annual Conference on Neural Information Processing Systems 2018, NeurIPS 2018, December 3-8, 2018, Montréal, Canada*, pp. 8580–8589, 2018. URL <https://proceedings.neurips.cc/paper/2018/hash/5a4be1fa34e62bb8a6ec6b91d2462f5a-Abstract.html>.

Karan, A. and Du, Y. Reasoning with sampling: Your base model is smarter than you think. *CoRR*, abs/2510.14901, 2025. doi: 10.48550/ARXIV.2510.14901. URL <https://doi.org/10.48550/arXiv.2510.14901>.

Kool, W., van Hoof, H., and Welling, M. Attention, learn to solve routing problems! In *7th International Conference on Learning Representations, ICLR 2019, New Orleans, LA, USA, May 6-9, 2019*. OpenReview.net, 2019. URL <https://openreview.net/forum?id=ByxBF8sRqYm>.

Lewkowycz, A., Andreassen, A., Dohan, D., Dyer, E., Michalewski, H., Ramasesh, V. V., Slone, A., Anil, C., Schlag, I., Gutman-Solo, T., Wu, Y., Neyshabur, B., Gur-Ari, G., and Misra, V. Solving quantitative reasoning problems with language models. In Koyejo, S., Mohamed, S., Agarwal, A., Belgrave, D., Cho, K., and Oh, A. (eds.), *Advances in Neural Information Processing Systems 35: Annual Conference on Neural Information Processing Systems 2022, NeurIPS 2022, New Orleans, LA, USA, November 28 - December 9, 2022*, 2022. URL http://papers.nips.cc/paper_files/paper/2022/hash/18abbeef8cfe9203fdf9053c9c4fe191-Abstract.html.

Liu, Z., Chen, C., Li, W., Qi, P., Pang, T., Du, C., Lee, W. S., and Lin, M. Understanding r1-zero-like training: A critical perspective. *CoRR*, abs/2503.20783, 2025. doi: 10.48550/ARXIV.2503.20783. URL <https://doi.org/10.48550/arXiv.2503.20783>.

Luo, M., Tan, S., Wong, J., Shi, X., Tang, W. Y., Roongta, M., Cai, C., Luo, J., Zhang, T., Li, L. E., et al. Deepscaler: Surpassing o1-preview with a 1.5 b model by scaling rl. *Notion Blog*, 2025.

Prabhudesai, M., Chen, L., Ippoliti, A., Fragkiadaki, K., Liu, H., and Pathak, D. Maximizing confidence alone improves reasoning. *CoRR*, abs/2505.22660, 2025. doi: 10.48550/ARXIV.2505.22660. URL <https://doi.org/10.48550/arXiv.2505.22660>.

Song, Y., Kempe, J., and Munos, R. Outcome-based exploration for LLM reasoning. *CoRR*, abs/2509.06941, 2025. doi: 10.48550/ARXIV.2509.06941. URL <https://doi.org/10.48550/arXiv.2509.06941>.

Wang, S., Yu, L., Gao, C., Zheng, C., Liu, S., Lu, R., Dang, K., Chen, X., Yang, J., Zhang, Z., Liu, Y., Yang, A., Zhao, A., Yue, Y., Song, S., Yu, B., Huang, G., and Lin, J. Beyond the 80/20 rule: High-entropy minority tokens drive effective reinforcement learning for LLM reasoning. *CoRR*, abs/2506.01939, 2025. doi: 10.48550/ARXIV.2506.01939. URL <https://doi.org/10.48550/arXiv.2506.01939>.

Wu, J., Huang, K., Wu, J., Zhang, A., Wang, X., and He, X. Quantile advantage estimation for entropy-safe reasoning. *CoRR*, abs/2509.22611, 2025. doi: 10.48550/ARXIV.2509.22611. URL <https://doi.org/10.48550/arXiv.2509.22611>.

Xiong, W., Yao, J., Xu, Y., Pang, B., Wang, L., Sahoo, D., Li, J., Jiang, N., Zhang, T., Xiong, C., and Dong, H. A minimalist approach to LLM reasoning: from rejection sampling to reinforce. *CoRR*, abs/2504.11343, 2025. doi: 10.48550/ARXIV.2504.11343. URL <https://doi.org/10.48550/arXiv.2504.11343>.

Yang, A., Li, A., Yang, B., Zhang, B., Hui, B., Zheng, B., Yu, B., Gao, C., Huang, C., Lv, C., Zheng, C., Liu, D., Zhou, F., Huang, F., Hu, F., Ge, H., Wei, H., Lin, H., Tang, J., Yang, J., Tu, J., Zhang, J., Yang, J., Yang, J., Zhou, J., Lin, J., Dang, K., Bao, K., Yang, K., Yu, L., Deng, L., Li, M., Xue, M., Li, M., Zhang, P., Wang, P., Zhu, Q., Men, R., Gao, R., Liu, S., Luo, S., Li, T., Tang, T., Yin, W., Ren, X., Wang, X., Zhang, X., Ren, X., Fan, Y., Su, Y., Zhang, Y., Zhang, Y., Wan, Y., Liu, Y., Wang, Z., Cui, Z., Zhang, Z., Zhou, Z., and Qiu, Z. Qwen3 technical report. *CoRR*, abs/2505.09388, 2025. doi: 10.48550/ARXIV.2505.09388. URL <https://doi.org/10.48550/arXiv.2505.09388>.

Yu, Q., Zhang, Z., Zhu, R., Yuan, Y., Zuo, X., Yue, Y., Fan, T., Liu, G., Liu, L., Liu, X., Lin, H., Lin, Z., Ma, B., Sheng, G., Tong, Y., Zhang, C., Zhang, M., Zhang, W., Zhu, H., Zhu, J., Chen, J., Chen, J., Wang, C., Yu, H., Dai, W., Song, Y., Wei, X., Zhou, H., Liu, J., Ma, W., Zhang, Y., Yan, L., Qiao, M., Wu, Y., and Wang, M. DAPO: an open-source LLM reinforcement learning system at scale. *CoRR*, abs/2503.14476, 2025. doi: 10.48550/ARXIV.2503.14476. URL <https://doi.org/10.48550/arXiv.2503.14476>.

Yue, Y., Chen, Z., Lu, R., Zhao, A., Wang, Z., Yue, Y., Song, S., and Huang, G. Does reinforcement learning really incentivize reasoning capacity in llms beyond the base model? *CoRR*, abs/2504.13837, 2025. doi: 10.48550/ARXIV.2504.13837. URL <https://doi.org/10.48550/arXiv.2504.13837>.

A. Proof of Theorem 2.1

Theorem A.1. *The maximizer of Equation (1), denoted as π^* , is given by*

$$\pi^*(o|q) = \frac{1}{Z(q)} \pi_{\text{ref}}(o|q) \exp\left(\frac{A(q, o)}{\beta}\right), \quad (5)$$

where $Z(q)$ is the partition function ensuring normalization.

Proof. Because the expectation over q is linear and the policy can depend arbitrarily on q , the maximization decomposes across queries. For each fixed q , we omit it from notation for brevity and can independently maximize the per-query objective as follows:

$$J(\pi) = \int \pi(o) A(o) do - \beta \int \pi(o) \log \frac{\pi(o)}{\pi_{\text{ref}}(o)} do.$$

We introduce a Lagrange multiplier λ for the normalization constraint:

$$\mathcal{L}[\pi, \lambda] = \int \pi(o) A(o) do - \beta \int \pi(o) \log \frac{\pi(o)}{\pi_{\text{ref}}(o)} do - \lambda \left(\int \pi(o) do - 1 \right).$$

Taking the functional derivative with respect to $\pi(o)$ (pointwise) yields:

$$\frac{\delta \mathcal{L}}{\delta \pi(o)} = A(o) - \beta \left(\log \frac{\pi(o)}{\pi_{\text{ref}}(o)} + 1 \right) - \lambda.$$

Setting the derivative to zero for every o gives:

$$A(o) - \beta (\log \pi(o) - \log \pi_{\text{ref}}(o) + 1) - \lambda = 0.$$

We rearrange the above equation and obtain:

$$\log \pi(o) = \log \pi_{\text{ref}}(o) + \frac{A(o)}{\beta} - \left(1 + \frac{\lambda}{\beta}\right).$$

We then exponentiate both sides:

$$\pi(o) = \pi_{\text{ref}}(o) \exp\left(\frac{A(o)}{\beta}\right) \exp\left(-1 - \frac{\lambda}{\beta}\right).$$

The factor $\exp(-1 - \lambda/\beta)$ is independent of o . Due to $\int \pi(o) do = 1$, we have:

$$\pi(o) = \frac{\pi_{\text{ref}}(o) \exp\left(\frac{A(o)}{\beta}\right)}{\int \pi_{\text{ref}}(o') \exp\left(\frac{A(o')}{\beta}\right) do'}.$$

Restoring the explicit dependence on q , we obtain Theorem 2.1. □

B. Distributional Update Geometry

Theorem B.1. *Consider a single gradient ascent step $\theta^+ = \theta + \eta \nabla_\theta \hat{J}(\theta)$ on the empirical objective with a learning rate of η . In the functional space of policies, let π_t denote the policy at step t . Under a first-order Taylor expansion, the updated policy π_{t+1} relates to the current policy π_t and the batch-optimal policy $\hat{\pi}$ as:*

$$\pi_{t+1}(o|q) \propto \pi_t(o|q)^{1-\eta\beta} \cdot \hat{\pi}(o|q)^{\eta\beta}. \quad (6)$$

Proof. The empirical objective $\hat{J}(\theta)$ is defined as:

$$\hat{J}(\theta) = \sum_i \frac{N_i}{G} A_i \log \pi_\theta(o_i) - \beta D_{KL}(\pi_\theta \| \pi_{\text{ref}}).$$

The batch-optimal policy $\hat{\pi}$ satisfies the stationary condition $\nabla_{\pi} \hat{J} = 0$, which yields $\hat{\pi}(o_i) = \frac{1}{Z'} \pi_{\text{ref}}(o_i) \exp(\frac{N_i A_i}{\beta G})$ according to ???. Taking the log:

$$\frac{N_i A_i}{\beta G} = \log \hat{\pi}(o_i) - \log \pi_{\text{ref}}(o_i) + \log Z'$$

The gradient of \hat{J} with respect to the log-probability $w_i = \log \pi_\theta(o_i)$ is:

$$\frac{\partial \hat{J}}{\partial w_i} = \frac{N_i A_i}{G} - \beta(\log \pi_\theta(o_i) - \log \pi_{\text{ref}}(o_i) + 1).$$

Combining the above two equations:

$$\frac{\partial \hat{J}}{\partial w_i} = \beta(\log \hat{\pi}(o_i) - \log \pi_{\text{ref}}(o_i) + \log Z') - \beta \log \pi_\theta(o_i) + \beta \log \pi_{\text{ref}}(o_i) - \beta = \beta(\log \hat{\pi}(o_i) - \log \pi_\theta(o_i)) + \text{constant}.$$

In functional space, the update in log-space is:

$$\log \pi_{t+1}(o_i) = \log \pi_t(o_i) + \eta \frac{\partial \hat{J}}{\partial w_i} = \log \pi_t(o_i) + \eta \beta(\log \hat{\pi}(o_i) - \log \pi_t(o_i)) + C.$$

Rearranging the terms:

$$\log \pi_{t+1}(o_i) = (1 - \eta \beta) \log \pi_t(o_i) + \eta \beta \log \hat{\pi}(o_i) + C$$

Exponentiating both sides yields the geometric mean:

$$\pi_{t+1}(o_i) \propto \pi_t(o_i)^{1-\eta\beta} \cdot \hat{\pi}(o_i)^{\eta\beta}.$$

□

C. Proof of Theorem 2.3

Proof. We first derive the first bound. By definition of $Z'(q)$ and partitioning modes into unsampled, correct, and incorrect sets, we have:

$$Z'(q) = \sum_{k \notin S^+ \cup S^-} \pi_{\text{ref}}(o_k | q) + \sum_{i \in S^+} \pi_{\text{ref}}(o_i | q) e^{\frac{N_i A_+}{\beta G}} + \sum_{j \in S^-} \pi_{\text{ref}}(o_j | q) e^{\frac{N_j A_-}{\beta G}}.$$

Using $e^x \geq 1 + x$, we obtain:

$$\begin{aligned} Z'(q) &\geq \sum_{k \notin S^+ \cup S^-} \pi_{\text{ref}}(o_k | q) + \sum_{i \in S^+} \pi_{\text{ref}}(o_i | q) \left(1 + \frac{N_i A_+}{\beta G}\right) + \sum_{j \in S^-} \pi_{\text{ref}}(o_j | q) \left(1 + \frac{N_j A_-}{\beta G}\right) \\ &= \sum_{\text{all } k} \pi_{\text{ref}}(o_k | q) + \frac{1}{\beta G} \left[A_+ \sum_{i \in S^+} N_i \pi_{\text{ref}}(o_i | q) + A_- \sum_{j \in S^-} N_j \pi_{\text{ref}}(o_j | q) \right] \\ &= 1 + \frac{1}{\beta G} \left[A_+ \sum_{i \in S^+} N_i \pi_{\text{ref}}(o_i | q) - |A_-| \sum_{j \in S^-} N_j \pi_{\text{ref}}(o_j | q) \right], \end{aligned}$$

which proves the first bound.

We now specialize to normalized binary advantages. Substitute $A_+ = (1 - p^+)/\sigma$ and $A_- = -p^+/\sigma$ into the above bound:

$$Z'(q) \geq 1 + \frac{1}{\beta G \sigma} \left[(1 - p^+) \sum_{i \in S^+} N_i \pi_{\text{ref}}(o_i | q) - p^+ \sum_{j \in S^-} N_j \pi_{\text{ref}}(o_j | q) \right].$$

Using $\sum_{i \in S^+} N_i = Gp^+$ and $\sum_{j \in S^-} N_j = G(1 - p^+)$, we can express the weighted averages:

$$\bar{\pi}^+ = \frac{\sum_{i \in S^+} N_i \pi_{\text{ref}}(o_i | q)}{\sum_{i \in S^+} N_i}, \quad \bar{\pi}^- = \frac{\sum_{j \in S^-} N_j \pi_{\text{ref}}(o_j | q)}{\sum_{j \in S^-} N_j}.$$

Then we have:

$$\begin{aligned} Z'(q) &\geq 1 + \frac{1}{\beta \sigma} \left[(1 - p^+) p^+ \bar{\pi}^+ - p^+ (1 - p^+) \bar{\pi}^- \right] \\ &= 1 + \frac{p^+ (1 - p^+)}{\beta \sigma} (\bar{\pi}^+ - \bar{\pi}^-). \end{aligned}$$

By definition,

$$\pi_{\min}^+ \leq \bar{\pi}^+, \quad \bar{\pi}^- \leq \pi_{\max}^-,$$

so

$$\bar{\pi}^+ - \bar{\pi}^- \geq \pi_{\min}^+ - \pi_{\max}^- = \Delta_\pi.$$

Therefore, we see:

$$Z'(q) \geq 1 + \frac{p^+ (1 - p^+)}{\beta \sigma} \Delta_\pi.$$

If $\Delta_\pi > 0$, the right-hand side is greater than 1. For any unsampled mode o_k with $N_k = 0$, Theorem 2.2 gives

$$\hat{\pi}(o_k | q) = \frac{\pi_{\text{ref}}(o_k | q)}{Z'(q)} < \pi_{\text{ref}}(o_k | q).$$

Thus, all unsampled modes are uniformly suppressed. \square

D. Background for Section 2.3

The derivation presented here is largely adapted from the Neural Tangent Kernel framework. We now provide the derivation for the parameter update form $\Delta\theta$ and the induced logit shift Δf used in the main text. This derivation relies on the local properties of the neural network function under small parameter updates. For a small optimization step, the change in the model parameters $\Delta\theta$ is small. Consequently, the change in the network output can be approximated by the first-order Taylor expansion around the current parameters θ :

$$f(x; \theta + \Delta\theta) \approx f(x; \theta) + \nabla_\theta f(x; \theta)^\top \Delta\theta.$$

Consider a training batch with target logit shifts given by the vector \mathbf{y} . To achieve this shift locally, the parameter update $\Delta\theta$ must satisfy the linearized constraint:

$$\mathbf{J}_q \Delta\theta = \mathbf{y},$$

where \mathbf{J}_q is the Jacobian matrix of the batch samples. Since the number of parameters is typically much larger than the batch size, this system is under-determined. Standard gradient-based optimizers naturally update the parameters within the subspace spanned by the data gradients (the row space of \mathbf{J}_q). This corresponds to finding the solution with the minimum Euclidean norm $\|\Delta\theta\|_2$, representing the steepest direction to fit the local target:

$$\Delta\theta = \arg \min_{\delta} \|\delta\|_2^2 \quad \text{s.t.} \quad \mathbf{J}_q \delta = \mathbf{y}.$$

The closed-form solution to this problem is given by the Moore-Penrose pseudoinverse:

$$\Delta\theta = \mathbf{J}_q^\top (\mathbf{J}_q \mathbf{J}_q^\top)^{-1} \mathbf{y}.$$

Here, the matrix $\mathbf{K}_{qq} = \mathbf{J}_q \mathbf{J}_q^\top$ captures the local alignment between gradients of the batch samples. Once $\Delta\theta$ is determined, the change in the logit value for any other query-output pair (q', o') is governed by the same local linearization:

$$\Delta f(q', o') \approx \nabla_\theta f(q', o')^\top \Delta\theta.$$

Substituting the expression for $\Delta\theta$, we obtain:

$$\Delta f(q', o') = \nabla_\theta f(q', o')^\top \mathbf{J}_q^\top (\mathbf{J}_q \mathbf{J}_q^\top)^{-1} \mathbf{y} = \mathbf{k}_{q'}^\top \mathbf{K}_{qq}^{-1} \mathbf{y},$$

where $\mathbf{k}_{q'} = \mathbf{J}_q \nabla_\theta f(q', o')$ represents the vector of gradient dot products (kernel values) between the new query and the training batch. This confirms that within a small update step, the propagation of probability mass is dictated by gradient similarity.

E. Proof of Theorem 2.4

Theorem E.1. Let $\mathcal{A}_{\text{sum}} \triangleq \sum_{s=1}^G y_s = \frac{1}{\beta G} \sum_{s=1}^G N_s |A(q, o^{(s)})|$. The induced logit shift $\Delta f(q', o')$ satisfies the following bounds based on whether o' appears in the training batch $\{o^{(i)}, i = 1, \dots, G\}$:

- If $o' \notin \{o^{(s)}\}_{s=1}^G$, the logit increase is upper-bounded by:

$$\Delta f(q', o') \leq \frac{\eta \rho_{\max} \mathcal{A}_{\text{sum}}}{\lambda_{\min} + (G-1)\rho_{\min}}.$$

- If $o' = o^{(k)}$ for some $k \in \{1, \dots, G\}$, the logit increase is lower-bounded by

$$\Delta f(q', o') = \Delta f(q', o^{(k)}) \geq \frac{\eta N_{o'} (\lambda_{\min} - \rho_{\min})}{\lambda_{\max} - \rho_{\max}} \left(y_k - \frac{\rho_{\max} \mathcal{A}_{\text{sum}}}{\lambda_{\max} + (G-1)\rho_{\max}} \right).$$

Proof. We define the dual coefficient vector $\boldsymbol{\alpha} = \mathbf{K}_{qq}^{-1} \mathbf{y}$. We proceed by first bounding the entries of $\boldsymbol{\alpha}$.

Step 1: Bounds on $\boldsymbol{\alpha}$. Let $\mathbf{M}(\lambda, \rho) = (\lambda - \rho) \mathbf{I} + \rho \mathbf{1} \mathbf{1}^\top$, where diagonal entries are $\lambda > 0$ and off-diagonal entries are $\rho > 0$. Consider $\boldsymbol{\alpha}(\lambda, \rho) = \mathbf{M}(\lambda, \rho)^{-1} \mathbf{y}$. Applying the Sherman-Morrison formula⁴, the inverse $\mathbf{M}(\lambda, \rho)^{-1}$ applied to \mathbf{y} yields:

$$\boldsymbol{\alpha}(\lambda, \rho) = \mathbf{M}(\lambda, \rho)^{-1} \mathbf{y} = \frac{1}{\lambda - \rho} \left(\mathbf{I} - \frac{\rho}{\lambda + (G-1)\rho} \mathbf{1} \mathbf{1}^\top \right) \mathbf{y}.$$

The k -th coefficient of $\boldsymbol{\alpha}(\lambda, \rho)$ is given by:

$$\alpha_k(\lambda, \rho) = \frac{1}{\lambda - \rho} \left(y_k - \frac{\rho \mathcal{A}_{\text{sum}}}{\lambda + (G-1)\rho} \right).$$

Summing over all k , the interaction terms cancel out, simplifying to a dependence on the total mass:

$$\sum_s \alpha_s(\lambda, \rho) = \mathbf{1}^\top \mathbf{M}(\lambda, \rho)^{-1} \mathbf{y} = \frac{\mathcal{A}_{\text{sum}}}{\lambda + (G-1)\rho}.$$

Utilizing non-negativity of y_i , the spectral lower bound $\mathbf{K}_{qq} \succeq \mathbf{M}(\lambda_{\min}, \rho_{\min}) \succ 0$ and the order-reversing property of the matrix inverse, the sum of the coefficients is upper-bounded:

$$\sum_{s=1}^G \alpha_s = \mathbf{1}^\top \mathbf{K}_{qq}^{-1} \mathbf{y} \leq \mathbf{1}^\top \mathbf{M}(\lambda_{\min}, \rho_{\min})^{-1} \mathbf{y} = \frac{\mathcal{A}_{\text{sum}}}{\lambda_{\min} + (G-1)\rho_{\min}}.$$

Similarly, we have:

$$\sum_{s=1}^G \alpha_s \geq \mathbf{1}^\top \mathbf{M}(\lambda_{\max}, \rho_{\max})^{-1} \mathbf{y} = \frac{\mathcal{A}_{\text{sum}}}{\lambda_{\max} + (G-1)\rho_{\max}}.$$

⁴ $(\mathbf{A} + \mathbf{u}\mathbf{v}^\top)^{-1} = \mathbf{A}^{-1} - \frac{\mathbf{A}^{-1}\mathbf{u}\mathbf{v}^\top\mathbf{A}^{-1}}{1 + \mathbf{v}^\top\mathbf{A}^{-1}\mathbf{u}}$.

For individual dual coefficients α_k , we have the following two-sided bounds:

$$\frac{1}{\lambda_{\max} - \rho_{\max}} \left(y_k - \frac{\rho_{\max} \mathcal{A}_{\text{sum}}}{\lambda_{\max} + (G-1)\rho_{\max}} \right) \leq \alpha_k \leq \frac{1}{\lambda_{\min} - \rho_{\min}} \left(y_k - \frac{\rho_{\min} \mathcal{A}_{\text{sum}}}{\lambda_{\min} + (G-1)\rho_{\min}} \right).$$

Step 2: Bounds on Logit Shift $\Delta f(q', o')$. The logit change is given by:

$$\Delta f(q', o') = \sum_s \alpha_s k((q', o'), (q, o^{(s)})).$$

According to Assumption 2.2, we have $[\mathbf{k}_{q'}]_s = k((q', o'), (q, o^{(s)})) \approx \eta K((q, o'), (q, o^{(s)}))$.

Case 1: $o' \notin \{o^{(s)}\}_{s=1}^G$. Intuitively, for any distinct modes $o_a \neq o_b$, their kernel similarity is bounded by ρ_{\max} . Intuitively, the batch $\{o^{(s)}\}$ captures the densest region of the optimization landscape, i.e., the high-probability modes that share the most structural features and thus exhibit the highest gradient overlap. Consequently, any unseen mode $o' \notin \{o^{(s)}\}$ resides in the distribution's tail and is expected to have a lower gradient correlation with the batch samples than the samples have with each other, ensuring the bound holds. Then, we have:

$$[\mathbf{k}_{q'}]_s = k((q', o'), (q, o^{(s)})) \approx \eta K((q, o'), (q, o^{(s)})) \leq \eta \rho_{\max}.$$

Using bounds derived in Step 1, we obtain:

$$\Delta f(q', o') \leq \sum_{s=1}^G \alpha_s (\eta \rho_{\max}) = \eta \rho_{\max} \sum_{s=1}^G \alpha_s \leq \frac{\eta \rho_{\max} \mathcal{A}_{\text{sum}}}{\lambda_{\min} + (G-1)\rho_{\min}}.$$

Case 2: $o' \in \{o^{(s)}\}_{s=1}^G$. Let $S_{o'} = \{s \mid o^{(s)} = o'\}$ be the set of indices where the sample o' appears in the batch, with cardinality $|S_{o'}| = N_{o'}$. The logit shift accumulates contributions from all $N_{o'}$ occurrences (self-terms) and the remaining $G - N_{o'}$ samples (cross-terms):

$$\Delta f(q', o') = \sum_{s \in S_{o'}} \alpha_s [\mathbf{k}_{q'}]_s + \sum_{s \notin S_{o'}} \alpha_s [\mathbf{k}_{q'}]_s.$$

To derive a lower bound, we assume the stiffest kernel parameters $(\lambda_{\max}, \rho_{\max})$ for α (minimizing gradient magnitude) and the loosest parameters $(\lambda_{\min}, \rho_{\min})$ for transfer. Substituting $[\mathbf{k}_{q'}]_k \geq \eta \lambda_{\min}$ and $[\mathbf{k}_{q'}]_j \geq \eta \rho_{\min}$:

$$\begin{aligned} \Delta f(q', o') &\geq \eta \lambda_{\min} \sum_{s \in S_{o'}} \alpha_s + \eta \rho_{\min} \sum_{s \notin S_{o'}} \alpha_s \\ &= \eta \lambda_{\min} \sum_{s \in S_{o'}} \alpha_s + \eta \rho_{\min} \left(\sum_{\text{all}} \alpha_s - \sum_{s \in S_{o'}} \alpha_s \right) \\ &= \eta (\lambda_{\min} - \rho_{\min}) \sum_{s \in S_{o'}} \alpha_s + \eta \rho_{\min} \mathcal{A}_{\text{sum}}. \end{aligned}$$

Next, we substitute the exact form of α_k derived in Step 1, using the stiff parameters λ_{\max} and ρ_{\max} :

$$\alpha_k \geq \frac{1}{\lambda_{\max} - \rho_{\max}} \left(y_k - \frac{\rho_{\max} \mathcal{A}_{\text{sum}}}{\lambda_{\max} + (G-1)\rho_{\max}} \right).$$

Summing this over the $N_{o'}$ indices in $S_{o'}$:

$$\sum_{s \in S_{o'}} \alpha_s \geq \frac{1}{\lambda_{\max} - \rho_{\max}} \left(\sum_{s \in S_{o'}} y_s - N_{o'} \frac{\rho_{\max} \mathcal{A}_{\text{sum}}}{\lambda_{\max} + (G-1)\rho_{\max}} \right).$$

Substituting this back into the logit shift equation and dropping the non-negative term $\eta \rho_{\min} \mathcal{A}_{\text{sum}}$:

$$\Delta f(q', o') \geq \frac{\eta N_{o'} (\lambda_{\min} - \rho_{\min})}{\lambda_{\max} - \rho_{\max}} \left(y_k - \frac{\rho_{\max} \mathcal{A}_{\text{sum}}}{\lambda_{\max} + (G-1)\rho_{\max}} \right).$$

□

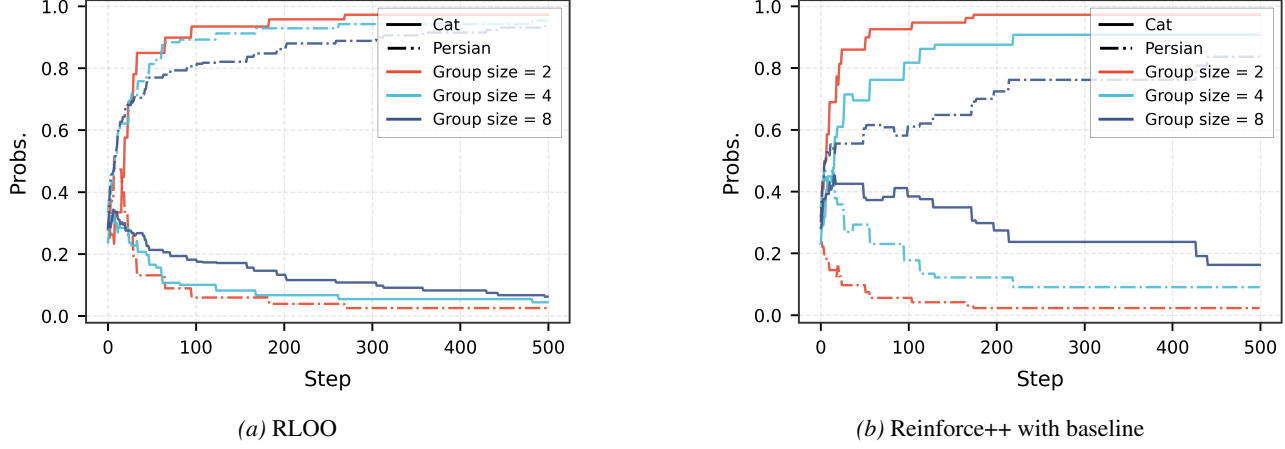


Figure 3. The effectiveness of RLOO and Reinforce++ with baseline on over-sharpening.

F. Proof of Corollary 2.2

Corollary F.1. Define the ratio \mathcal{R} of the lower bound in Case 2 to the upper bound in Case 1:

$$\mathcal{R} \triangleq \frac{\lambda_{\min} - \rho_{\min}}{\lambda_{\max} - \rho_{\max}} \cdot \left[\frac{N_{o'} y_k}{\mathcal{A}_{\text{sum}}} \cdot \left(\frac{\lambda_{\min} + (G-1)\rho_{\min}}{\rho_{\max}} \right) - \frac{\lambda_{\min} + (G-1)\rho_{\min}}{\lambda_{\max} + (G-1)\rho_{\max}} \right].$$

Under the assumption of a well-conditioned kernel (where $\lambda_{\min} \approx \lambda_{\max} \approx \lambda$ and $\rho_{\min} \approx \rho_{\max} \approx \rho$), this ratio simplifies to:

$$\mathcal{R} \approx N_{o'} \left[\frac{y_k}{\mathcal{A}_{\text{sum}}} \left(\frac{\lambda}{\rho} + G - 1 \right) - 1 \right].$$

Proof. Dividing the lower bound of Case 2 by the upper bound of Case 1 in Theorem 2.4:

$$\begin{aligned} \mathcal{R} &= \frac{\frac{\eta N_{o'} (\lambda_{\min} - \rho_{\min})}{\lambda_{\max} - \rho_{\max}} \left(y_k - \frac{\rho_{\max} \mathcal{A}_{\text{sum}}}{\lambda_{\max} + (G-1)\rho_{\max}} \right)}{\frac{\eta \rho_{\max} \mathcal{A}_{\text{sum}}}{\lambda_{\min} + (G-1)\rho_{\min}}} \\ &= \frac{\lambda_{\min} - \rho_{\min}}{\lambda_{\max} - \rho_{\max}} \cdot \left[\frac{N_{o'} y_k}{\mathcal{A}_{\text{sum}}} \cdot \left(\frac{\lambda_{\min} + (G-1)\rho_{\min}}{\rho_{\max}} \right) - \frac{\lambda_{\min} + (G-1)\rho_{\min}}{\lambda_{\max} + (G-1)\rho_{\max}} \right]. \end{aligned}$$

Assuming uniform parameters λ and ρ , the stiffness damping factor $\frac{\lambda - \rho}{\lambda + \rho}$ becomes 1. The common term η cancels out. We are left with:

$$\mathcal{R} \approx \frac{N_{o'} \left(y_k - \frac{\rho \mathcal{A}_{\text{sum}}}{\lambda + (G-1)\rho} \right)}{\frac{\rho \mathcal{A}_{\text{sum}}}{\lambda + (G-1)\rho}} = N_{o'} \left[\frac{y_k}{\mathcal{A}_{\text{sum}}} \left(\frac{\lambda}{\rho} + G - 1 \right) - 1 \right].$$

□

G. Supplementary Experiment for Section 2.4

Advanced Advantage Estimators. To ensure that the phenomenon of over-sharpening is not an artifact of simplistic advantage estimation, we extend our analysis to include RLOO and Reinforce++ with baseline. As illustrated in Figure 3, while these methods can slightly delay the onset of collapse compared to raw rewards, the policy eventually collapses onto a single mode.

Optimizer effect. As shown in Figure 4, both Momentum optimizer and AdamW optimizer significantly accelerate the rate of collapse compared to standard SGD. We see that, for Momentum optimizer, the policy collapses almost instantaneously

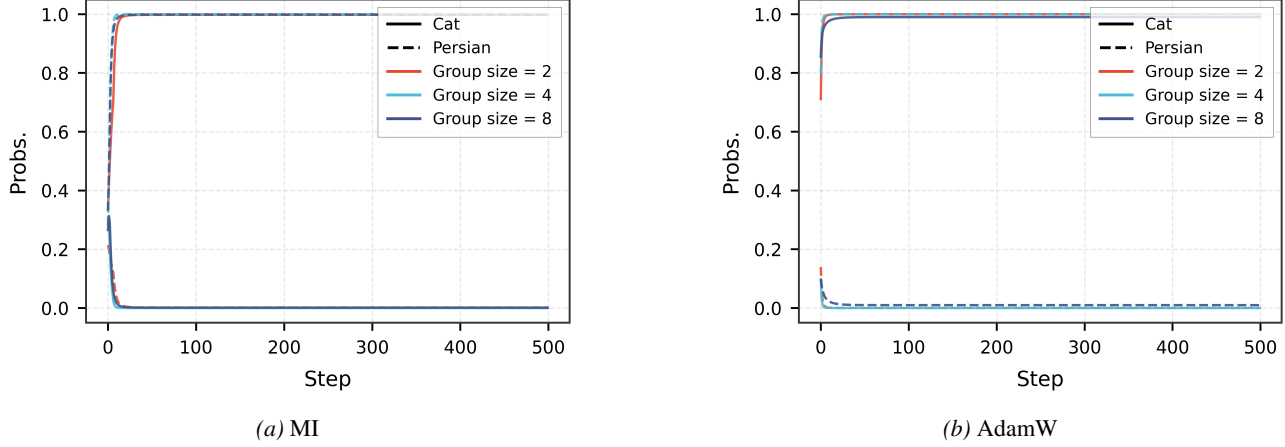


Figure 4. Effect of different optimizers on over-sharpening.

(within 20 steps) regardless of group size. This occurs because the momentum buffer accumulates gradients from early samples. Once sampling bias creates a slight preference for one mode (e.g., Cat), the history buffer sustains the update direction even if subsequent batches are more balanced. For AdamW optimizer, we observe a worse trend. By normalizing updates based on the second moment of the gradients, AdamW amplifies the effective learning rate, allowing the model to maximize the likelihood of the initially sampled modes more aggressively.

Kernel similarity. In Section 2.3, we establish that the propagation of collapse is governed by the ratio \mathcal{R} , which is heavily influenced by the ratio λ/ρ . To quantify this in our toy model, we calculate the dot products of the embeddings to approximate the kernel entries $K_{qq} \approx e_q^\top e_{q'}$. We study three degrees of similarity between the training query ($q = \text{Persian}$) and the held-out query ($q' = \text{Siamese}$), corresponding to the High, Mid, and Low similarity settings described in Section 2.4. The fixed embedding for Persian is $e_{\text{Persian}} = [0.75, 0.5, 0.25, 0.1]$. The similarity metrics are calculated as follows:

1. High Similarity:

- $e_{\text{Siamese}} = [0.25, 0.5, 0.75, 0.1]$.
- Self-similarity ($\lambda \approx \|e_{\text{Persian}}\|^2$): 0.8775.
- Cross-similarity ($\rho \approx e_{\text{Persian}}^\top e_{\text{Siamese}}$): $0.75(0.25) + 0.5(0.5) + 0.25(0.75) + 0.1(0.1) = 0.635$.
- Ratio (λ/ρ): 1.38.

2. Mid Similarity:

- $e_{\text{Siamese}} = [0.1, 0.5, 0.9, 0.1]$.
- Cross-similarity: $0.75(0.1) + 0.5(0.5) + 0.25(0.9) + 0.1(0.1) = 0.56$.
- Ratio (λ/ρ): 1.57.

3. Low Similarity:

- $e_{\text{Siamese}} = [0.0, 0.5, 1.0, 0.1]$.
- Cross-similarity: $0.75(0.0) + 0.5(0.5) + 0.25(1.0) + 0.1(0.1) = 0.51$.
- Ratio (λ/ρ): 1.72.

These calculations demonstrate that as the embeddings become less similar (moving from High to Low), the cross-similarity ρ decreases, causing the ratio λ/ρ to increase. A higher λ/ρ implies weaker semantic coupling, meaning updates to Persian have less impact on Siamese. This aligns with the empirical results in Figure 2, where the "High Similarity" setting (lowest λ/ρ) exhibited the most rapid degradation of accuracy on the held-out class.

Algorithm 1 Inverse-success Advantage Calibration + Distribution-Level Calibration

Require: policy π_θ , reference π_{ref} , optional memory m_ϕ , batch size B , group size G , calibration strength α , memory weight μ

- 1: **while** not converged **do**
- 2: Sample a mini-batch of queries $\{q_b\}_{b=1}^B$ from \mathcal{D} ;
- 3: **for** each query q_b **do**
- 4: **if** memory m_ϕ is used **then**
- 5: Compute calibrated logits $\tilde{f}(q_b, \cdot) = f_\theta(q_b, \cdot) - \mu f_\phi(q_b, \cdot)$;
- 6: Sample G trajectories $\{o_{b,s}\}_{s=1}^G \sim \text{softmax}(\tilde{f}(q_b, \cdot))$;
- 7: **else**
- 8: Sample G trajectories $\{o_{b,s}\}_{s=1}^G \sim \pi_\theta(\cdot | q_b)$;
- 9: **end if**
- 10: Compute verifiable rewards $r_{b,s}$ and advantages $A_{b,s}$;
- 11: Identify positive indices $S_b^+ = \{s : A_{b,s} > 0\}$, negatives S_b^- ;
- 12: Compute success count $|S_b^+|$;
- 13: **for** $s \in S_b^+$ **do** ▷ inverse-success calibration
- 14: $\tilde{A}_{b,s} \leftarrow A_{b,s} \cdot (G - |S_b^+|)^\alpha$;
- 15: **end for**
- 16: **for** $s \in S_b^-$ **do** ▷ leave negatives unscaled
- 17: $\tilde{A}_{b,s} \leftarrow A_{b,s}$;
- 18: **end for**
- 19: **end for**
- 20: Update θ using calibrated advantages $\tilde{A}_{b,s}$ and KL regularization to π_{ref} ;
- 21: **if** memory m_ϕ is used **then**
- 22: Update m_ϕ on sampled $(q_b, o_{b,s})$ pairs to track empirical frequencies;
- 23: **end if**
- 24: **end while**

Table 5. Sensitivity of IAC to the calibration strength α . We report AVG@8 and PASS@8 on Math500 and O-Bench for Qwen3-8B when varying α in IAC. When $\alpha = 0$, IAC reduces to the vanilla GRPO objective. We also include a simple filtering-based baseline that discards the easiest 25% of training queries according to their empirical success rate.

Metric	Dataset	0	0.5	1	1.5	2	Filtering-based
AVG@8	Math500	85.81	87.45	87.67	86.64	86.29	86.13
	O-Bench	49.79	50.47	50.49	52.11	50.17	50.21
PASS@8	Math500	91.39	93.79	94.54	94.37	93.85	92.06
	O-Bench	56.88	57.56	58.48	59.66	58.88	57.30

H. Supplementary Material for Section 3

Algorithm 1 summarizes the complete pipeline of our methods.

We validate the efficacy of our proposed calibration mechanisms using the toy setting described in Section 2.4. Figure 5 presents the evolution of probability mass. We see that inverse-success advantage calibration alone significantly retards the rate of collapse compared to the uncalibrated baseline. Coupling this with distribution-level calibration (memory network) enables the policy to reach a stable equilibrium where diversity is maintained, effectively arresting over-sharpening. Moreover, despite AdamW’s tendency to accelerate collapse, our methods still can prevent the aggressive elimination of alternative modes.

I. Supplementary Experiment for Section 4

Sensitivity to the calibration strength α . Table 5 investigates how α in IAC affects downstream performance on Math500 and O-Bench. Recall that α controls how strongly we up-weight advantages from hard, low-success queries and down-weight those from easy, high-success ones. When $\alpha = 0$, our method reduces exactly to GRPO, and the results at this setting coincide with the GRPO baseline. As α increases from 0 to 1, we observe a consistent improvement on both datasets: AVG@8 and PASS@8 on Math500 peak at $\alpha = 1$, while O-Bench attains its best PASS@8 at a slightly larger $\alpha = 1.5$. Beyond this moderate regime, further increasing α leads to mild degradation. Intuitively, small α under-corrects sampling

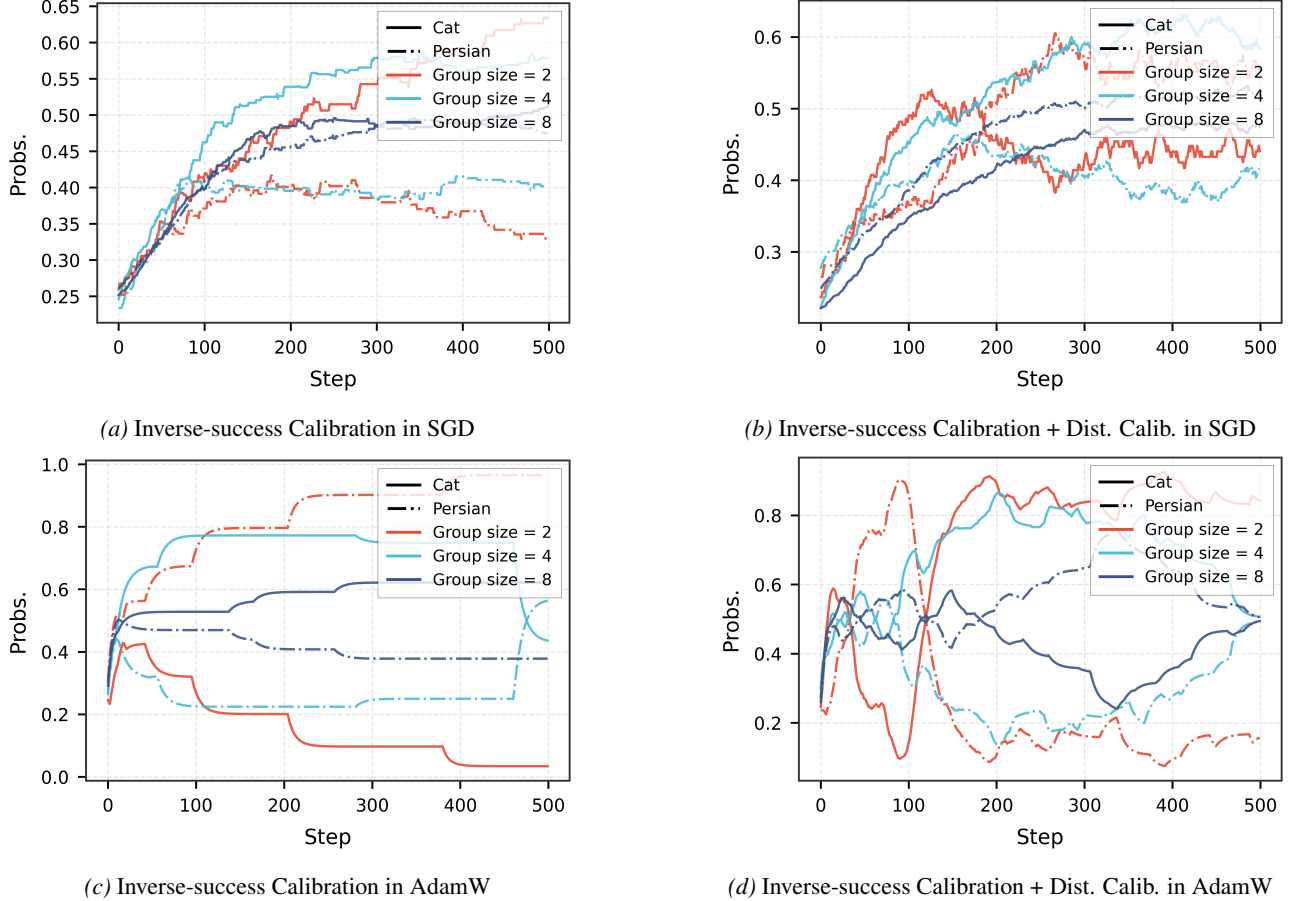


Figure 5. We apply our proposed mitigations to the Softmax example. The left column (a, c) employs only inverse-Success advantage calibration, showing a delayed rate of collapse. The right column (b, d) incorporates distribution-level calibration (memory network, $\mu = 0.5$), which arrests collapse and maintains diversity, even under the aggressive updates of AdamW.

bias, allowing easy queries to keep dominating the update and driving over-sharpening. In contrast, large α over-corrects, overly suppressing signal from already-mastered queries and making the optimization less sample-efficient. As we can see, $\alpha = 1$ appears to be a good choice in practice.

Table 5 also compares IAC against a filtering strategy that discards the easiest 25% of training queries according to their empirical success rate. Across both Math500 and O-Bench, filtering yields only modest gains over GRPO and is consistently weaker than IAC. This gap highlights a key limitation of hard filtering: removing easy queries entirely reduces the effective training distribution and discards useful gradient information, particularly about how to maintain correctness on already-solved patterns. IAC, in contrast, keeps all queries in the optimization loop but rescales their influence on the update. Easy queries contribute a smaller—but non-zero—signal, preventing them from overwhelming the batch partition function $Z'(q)$, while hard queries are emphasized in a smooth, data-dependent manner. From a distributional perspective, filtering crudely prunes regions of the solution space, whereas IAC gently rebalances probability mass across difficulty levels. The latter is more effective at preserving useful behaviors on easy instances while still allocating sufficient capacity to explore and stabilize difficult, low-success regimes, which explains the consistent empirical advantage of IAC over filtering-based baselines.

Entropy evolution. Figure 6 tracks the evolution of the policy entropy when applying DAPO alone versus DAPO combined with IAC. Both methods start from similar initial entropy, but their trajectories diverge markedly over training. Under plain DAPO, entropy decreases monotonically and eventually settles around 0.08, signalling that the policy becomes almost deterministic. In contrast, for DAPO+IAC, it stabilizes at a much higher level, fluctuating between 0.20 and 0.24 throughout training. This indicates that the policy retains a substantial degree of stochasticity and continues to explore multiple semantic

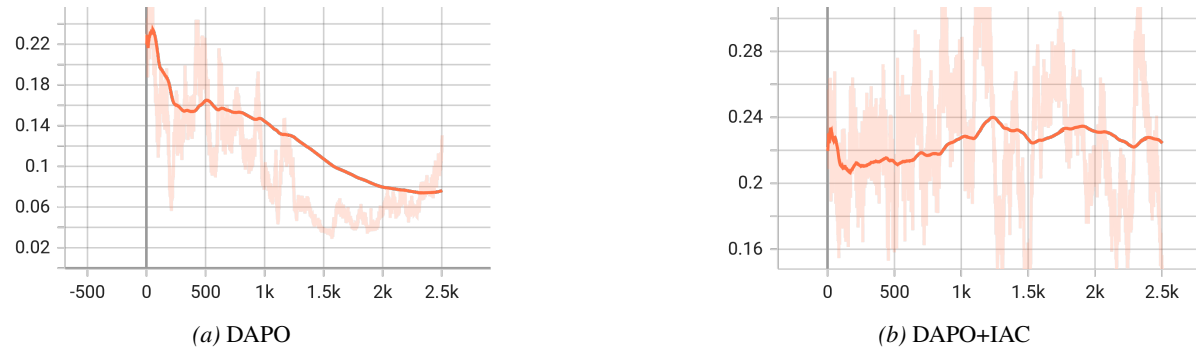


Figure 6. Evolution of policy entropy under DAPO and DAPO+IAC.

modes even late in optimization.